FINAL PERFORMANCE REPORT

Introduction

Through billions of years of evolution, nature has produced a plethora of biomaterials with a vast range of truly remarkable properties from serving as protection and when compromised self-heal to harnessing to exhibiting extreme strength and load bearing properties. Our lab exploits the protein elements that are involved in such biomaterials to fabricate unique hybrids or protein block polymers that we anticipate will share the materials properties of the biomaterials in which they are based. The biomaterials are generated biosynthetically and thus we are able to control the polymer composition, length and molecular structure on the nm scale. Here we biosynthesize and characterize a set of designed protein block polymers for assembly. Our long-term goal is to predictably design novel biopolymer materials with precisely controlled physico-chemical properties to address significant problems in biotechnology, biomolecular and bioelectronics design.

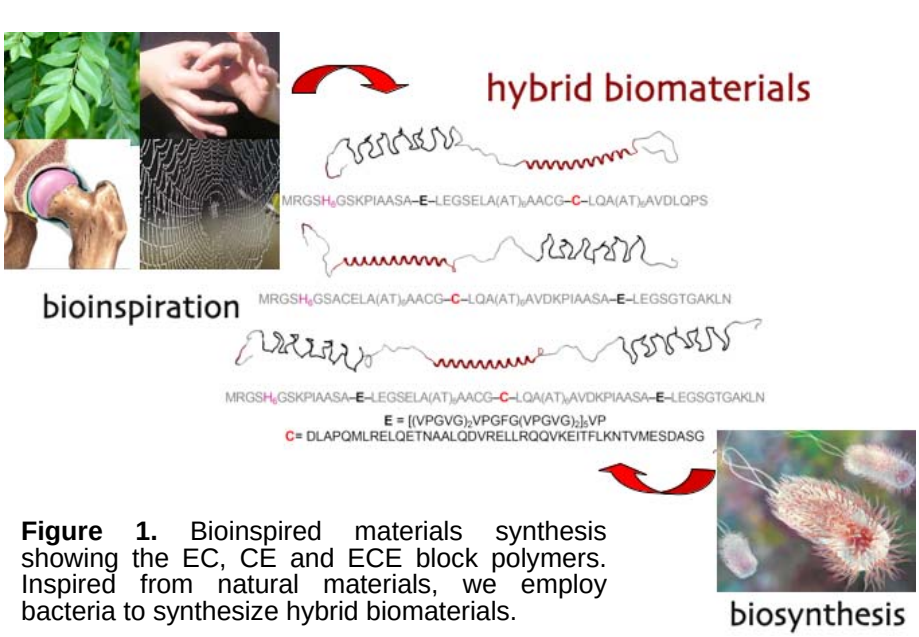

Figure 1. Bioinspired materials synthesis showing the EC, CE and ECE block polymers. Inspired from natural materials, we employ bacteria to synthesize hybrid biomaterials.

Essentially, we have generated hybrids from protein comprised of *two distinct* self-assembling domains (SADs): elastin (E) and cartilage oligomeric matrix protein coiled-coil (COMPcc, C). Elastin is an important class of structural proteins that is responsible for the elastic properties of tissues. Elastins are comprised of a pentapeptide $(VPGXG)_n$ repeat, which self-assemble to form a helical β-spiral that endows it with its elastic character (Figure 1).[1] Unlike most polymers, elastin exhibits inverse temperature behavior, which classifieds them as "smart" material. By varying the identity of X as well as the number of repeats (n), it is possible to tune the temperature transition.[2] Due to this unique property, they are easily purified and serve as excellent scaffolds. By contrast, COMP is a non-collagenous protein identified in cartilage, tendon and ligament.[3] Although it is comprised of various domains, it is assembled into a homopentamer via an N-terminal coiled-coil domain (COMPcc) (Figure 1). COMPcc possesses a hydrophobic pore that is 7.3 nm long with a diameter of 0.2-0.6 nm.[4] Recent structural studies reveal that the hormone 1,25-dihydroxyvitamin D3 (vit D) can bind in

REPORT DOCUMENTATION PAGE

Form Approved
OMB No. 0704-0188

1. REPORT DATE *(DD-MM-YYYY)*	2. REPORT TYPE	3. DATES COVERED *(From - To)*
05/31/2010	Final Technical Report	01/01/2007-05/31/2010

4. TITLE AND SUBTITLE
Engineered Protein Polymers

5a. CONTRACT NUMBER

5b. GRANT NUMBER
FA9550-07-1-0060

5c. PROGRAM ELEMENT NUMBER

6. AUTHOR(S)
Jin K. Montclare

5d. PROJECT NUMBER

5e. TASK NUMBER

5f. WORK UNIT NUMBER

7. PERFORMING ORGANIZATION NAME(S) AND ADDRESS(ES)

Polytechnic Institute of New
York University
6 Metrotech Center
Brooklyn, NY 11201

8. PERFORMING ORGANIZATION REPORT NUMBER

9. SPONSORING / MONITORING AGENCY NAME(S) AND ADDRESS(ES)
Air Force Office of Sci. Res.
875 North Randolph Street
Suite 325, Rm 3112
Arlington, VA 22203

10. SPONSOR/MONITOR'S ACRONYM(S)

11. SPONSOR/MONITOR'S REPORT NUMBER(S)

12. DISTRIBUTION / AVAILABILITY STATEMENT

Distribution A -- approved for public release; unlimited distribution

13. SUPPLEMENTARY NOTES

14. ABSTRACT

We have developed protein block polymers as well as homopolymers comprised cartilage oligomeric matrix protein coiled coil (C) and elastin (E). Three fusion—EC, CE and ECE—have been biosynthesized and characterized for their physicochemical properties in addition to the homopolymers. Depending on the orientation and the number of blocks, we discover that the secondary structure and supramolecular assemblies vary. In general, the block polymers assembled into particles that presented different mechanical properties. The C homopolymer, however, is able to assemble into fibers in a metal dependent fashion. Finally, we demonstrate that we can control the thermoresponsive behavior of the block polymer through the control of the E domain length.

15. SUBJECT TERMS

16. SECURITY CLASSIFICATION OF:			17. LIMITATION OF ABSTRACT	18. NUMBER OF PAGES	19a. NAME OF RESPONSIBLE PERSON
a. REPORT	b. ABSTRACT	c. THIS PAGE			Jin K Montclare
U	U	U	UU		19b. TELEPHONE NUMBER *(include area code)* 718-260-3679

the pore.[4] This, in addition to other biochemical studies, suggests that the role of the pentameric coiled-coil is to store vit D for signaling events during morphogenesis and repair of cartilage and bone.[5] This ability to house a small molecule in the pore of the protein represents an important feature that may be exploited to assist in self-assembly or to house and deliver small molecules.

The protein block polymers are fused in 2 orientations (EC and CE) and a final construct in which an additional E block is appended (ECE) (Figure 1). The following are the sequences of the E $((VPGVP)_2(VPGFG)(VPGVG)_2)_2$ and C (DLAPQMLRELQETNAALQDVRELLRQQVKEITFLKNTVMESDASG) blocks. We choose to engineer in an N-terminal His-tag to each protein construct for facile purification. These biomaterials are synthesized using bacteria that have been programmed with appropriate genes that encode the protein elements.

Originally in the proposed grant, the following aims were proposed.

Aim 1: To generate protein polymer constructs, genetic engineering techniques will be employed. Specifically, three EC, CE and ECE copolymers alongside the E and C homopolymer controls will be created.

Aim 2: To produce sufficient quantities of each construct, proteins will be overexpressed using *E. coli*. The resulting polymers will be purified and characterized for mondispersity by MALDI-TOF analysis.

Aim 3: To characterize the structure and aggregation properties of each polymer as a function of temperature, pH and salt conditions via CD, SEC, MALLS, viscometry, AFM and TEM.

Aim 4: To investigate whether there is a dependence of polymer structure and behavior on small molecule, the protein polymers will be characterized for binding and release using fluorescence measurements.

Aim 5: From our understanding of the physical characteristics of each pure polymer, we plan to combine the various polymer solutions in different ratios to tune the composition and physico-chemical properties of the bulk polymer.

We completed nearly all of the aims and also accomplished the following aims.

Aim 6: To generate and characterize single-alanine mutations of the C homopolymer. Residues important for structure, self-assembly and small molecule recognition will be indentified.

Aim 7: To investigate the templation of metal nanoparticles as well as soluble metal dependent assembly on the C homopolymer.

Aim 8: To fabricate a library of E_nC and CE_n diblocks in which the E domains are truncated to control the temperature-dependent assembly.

Results in Relationship to Aims

Aim 1. The design of the DNA construct relied on first cloning in the C gene into a plasmid with sufficient restriction sites that flank each side of the gene. The incorporation of unique restriction sites later enabled the incorporation of the E domain either N- or C-terminally or both to the C domain, maintaining the modularity of the entire construct. To allow for pentamer assembly of C, linkers $A_2(TA)_6$ on the 5'end and $A_2(TA)_7$ on the 3'end of the gene were introduced (Figure 1). The C insert bearing the linkers was generated via PCR assembly and successfully restricted with SacI and SalI, leading to a 236 base pair gene. This was then ligated into PQE30 (Qiagen) to generate pQE30/C. The E domain was PCR amplified and cloned in N- or C-terminally to pQE30/C to generate pQE30/CE, pQE30/EC and pQE30/ECE. As a control, pQE30/E was also produced. All constructs were confirmed via DNA sequencing analysis.

Aim 2. All proteins were expressed and purified using the vectors above. Protein polymers were purified under denaturing conditions using a Ni or Co column via FPLC.**(r)** Briefly, proteins were expressed in a 2L flask containing 200 mL of M9 minimal medium with 200 µL of each of the following: 1M $MgSO_4$, 0.1M $CaCl_2$, 35 mg/ mL chloramphenicol, 200 mg/ mL ampicillin, and 35 mg/ mL vitamin B. The M9 medium also contained 8 mL of 1g/L 20 amino acid solution and 2 mL of a 40% glucose solution. After 6 hours of pre-induction at 37°C and 350 rpm an OD_{600} of 1.0 was reached. The cell culture was then centrifuged at 4000 rpm and cell pellet was washed twice with cold 0.9% NaCl and then re-suspended in a 2L flask with 200 mL fresh M9 medium containing all the ingredients above with 200 µL of 200 mg/ mL isopropyl beta-D-1-thiogalactopyranoside. Expression was induced for 3 hours at 37°C and 350 rpm. Cells were centrifuged at 8000 rpm, and stored in the -80°C. Cells were subjected to osmotic shock and then lysed via French press at 23600 psi. To remove cell debris, samples were centrifuged at 20,000 RCF at 4°C. The proteins in the supernatant was purified under denaturing conditions via IMAC HighTrap FF column (GE Life Sciences) on FPLC and were eluted in 50 mM sodium phosphate dibasic and 6M urea pH = 8.0 with an imidazole gradient from 20 mM to 1 M across 10 mL. The molar masses of EC, CE and ECE were 22731 Da, 22911 Da and 35188 Da, respectively. Although SDS-PAGE analysis of the purified polymers revealed a slightly higher molecular weight for EC, CE and ECE (Figure 2), due to the E portion of the block polymers, the exact masses and polymer monodispersity were confirmed by MALDI.[6]

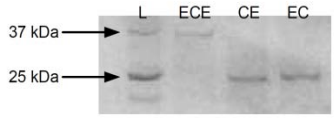

Figure 2. SDS PAGE of purified EC, CE and ECE.

Aim 3. To determine the conformations of the protein polymers, far UV circular dichroism (CD) experiments were conducted. As a control, the homopolymers C and E were monitored; C exhibited a helical structure that transitioned to random coil as the temperature was raised, while E showed an initial beta-conformation that slightly

decreased in value at higher temperatures. The following block polymer secondary structure contributions were assessed using SELCON3. Although nearly identical in composition, the EC and CE diblocks differed in secondary structure and exhibited

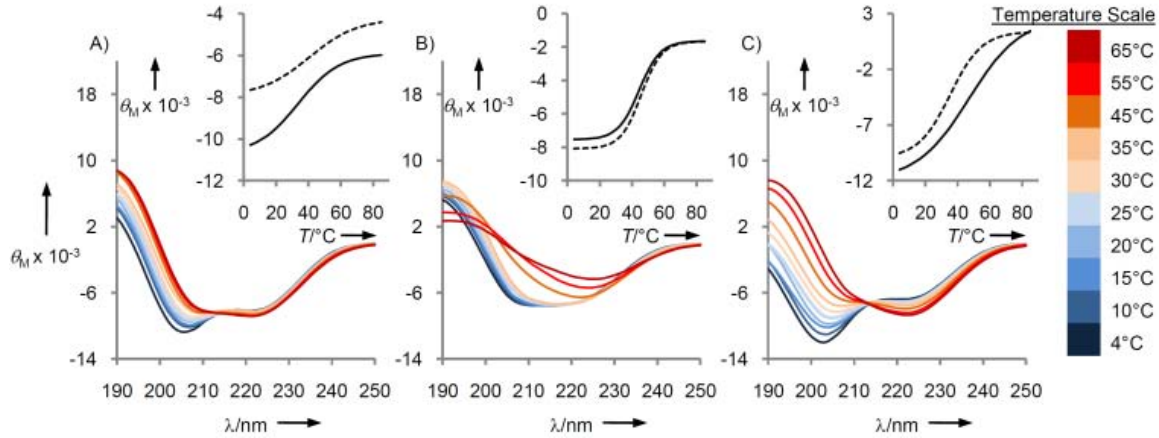

Figure 3. CD wavelength scans of a) EC, b) CE, and c) ECE as a function of temperature. Shown are the melt curves for the constructs as a function of fraction folded. Shown as insets are the melt curves for the constructs in the absence (solid line) and presence (broken line) of vD at a) EC, b) CE, and c) ECE

distinct temperature dependent conformational changes (Figures 3a, b). In the case of EC, a random like structure was observed at low temperatures, which then shifted into a predominantly helical and beta-conformation, with a calculated melting temperature (T_m) of 33°C (Figure 3a). The CE diblock revealed an overall random and beta-structure at low temperatures that transitioned into a red-shifted single minimum indicative of a predominantly beta-conformation, with a T_m of 44°C (Figure 3b). The ECE triblock demonstrated a similar random-like conformation as the EC diblock at low temperatures. Upon increase in temperature, ECE transitioned into a helix and finally to a beta-conformation with a T_m of 47°C (Figure 3c). The presence of the additional E domain not only increased the melting temperature, but also facilitated the formation of a beta-conformation at high temperatures. Essentially, the overall polymer conformation was strongly influenced by the N-terminal fusion and the number of blocks.[6]

An important feature of COMPcc is that it is able to bind vitamin D_3 (vD) in the hydrophobic pore of the pentameric coiled- coil. In fact, the crystal structure demonstrates the binding of two vD molecules in the pore[9]. Moreover, CD analysis reveals that for C in the presence of vD, a 6°C increase in T_m is observed, while in contrast, E shows a 10°C decrease in T_m with vD. The EC diblock incubated with vD shows a less random conformation at low temperatures with a $[\theta]_{222}/[\theta]_{208}$ of 0.83 relative to the unbound polymer (0.79). An increase in T_m by 6.9°C is observed for EC in the presence of vD, indicating that the small molecule is binding to the polymer (Figure 3a). The CE diblock bound to vD demonstrates a slightly less random with a $[\theta]_{222}/[\theta]_{208}$ of 1.0 from 0.96 when unbound; SELCON analysis reveals a beta-structure upon increase in temperature. The polymer exhibits a modest enhancement in T_m by 1.3°C in the presence of vD (Figure 3b). Like the EC diblock, the ECE triblock with vD reveals a less random

conformation with a $[\theta]_{222}/[\theta]_{208}$ of 0.72 relative to the unincubated polymer (0.68). The addition of vD to ECE results in a loss in the isosbestic point in which the final structure at the highest temperature is predominantly a β-conformation with a single minimum at 222 nm. This shift in conformation is expressed by a large decrease in T_m by 10.7°C, in contrast to the previous 2 diblocks (Figure 3c). In this case, the vD accelerates the conformational change from random to coil to β-structure and is doing so in a more cooperative fashion as demonstrated by the highly sigmoidal curve, similar to the E homopolymer in the presence of vD (Figure 3c). For all three polymers, vD influences their microstructures in which the overall conformation and melt is altered, with an acceleration of β-conformation formation at elevated temperatures.

In addition to structural information, we have investigated the self-assembly of these block copolymers with dynamic light scattering (DLS, probing sizes comparable to or less than hundreds of nm, Figure 4) and small angle light scattering (SALS, for sizes larger than hundreds of nm). The C domains are known to form pentamers, [4]while the E

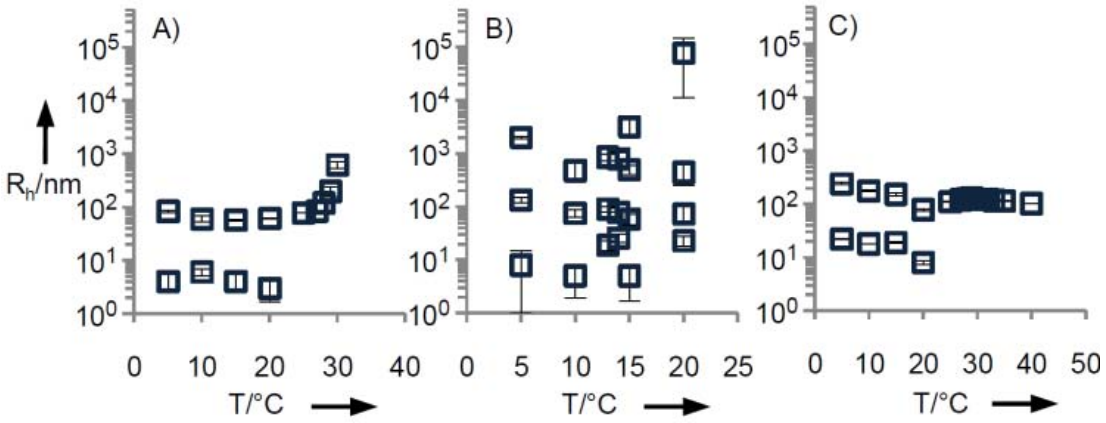

Figure 4. Hydrodynamic radius of A) EC, B) CE, and C) ECE as a function of temperature derived from DLS.

assembles into beta-spiral aggregates.[7,8] The EC shows two DLS modes below T_t ~25°C and one mode above T_t. At lower temperatures the two modes correspond to the unaggregated monomers (hydrodynamic radius, R_h ~ 4 nm) and aggregates with average R_h decreasing from 85 nm to 60 nm with temperature. At higher temperatures, there is only one mode representing aggregates with R_h increasing with temperature (Figure 4A). At even higher temperatures, the aggregates are much bigger to be determined by DLS. However, the SALS shows that a characteristic length of ~21 μm is spontaneously selected and that the scattered intensity increases with time suggesting the spinodal decomposition of phase separation. The DLS behavior of CE is qualitatively different from that of EC. There are more than two DLS modes, although the sizes of aggregates corresponding to the first two modes are comparable (Figure 4B) to those of EC. The additional modes in DLS indicate that the aggregates are polydisperse with sizes larger than those measurable with DLS and increasing with time. This is further supported by SALS where scattered intensity grows with time.[12] The ECE triblock exhibits a bimodal behaviour below T_t ~ 25°C, and only one aggregated structure above the T_t (Figure 4C).

The R_h of the aggregate (slow mode) decreases as the T_t is approached. The R_h of the fast mode remains at ~ 20 nm below the T_t. Above the T_t, there is only one mode with an R_h of 125 nm. Unlike the two diblocks, SALS experiments do not show any micron-scale features at temperatures above the T_t. Thus, the overall macroscopic assembly of the polymer is dependent on the block orientation and number.[6]

Transmission electron microscopy (TEM) analysis were performed to visualize the morphologies of each block polymer. We confirmed the formation of particles for all protein polymers (Figure 5). The homopolymers E and C as well as the non-covalent mixture of E+C were examined as controls. The E homopolymer illustrated the smallest particles with an average diameter size of 18.1 ± 3.7 nm, while C revealed significantly larger particles of 30.4 ± 5.8 nm (Figure 5a, b). The E+C mixture possessed particles with

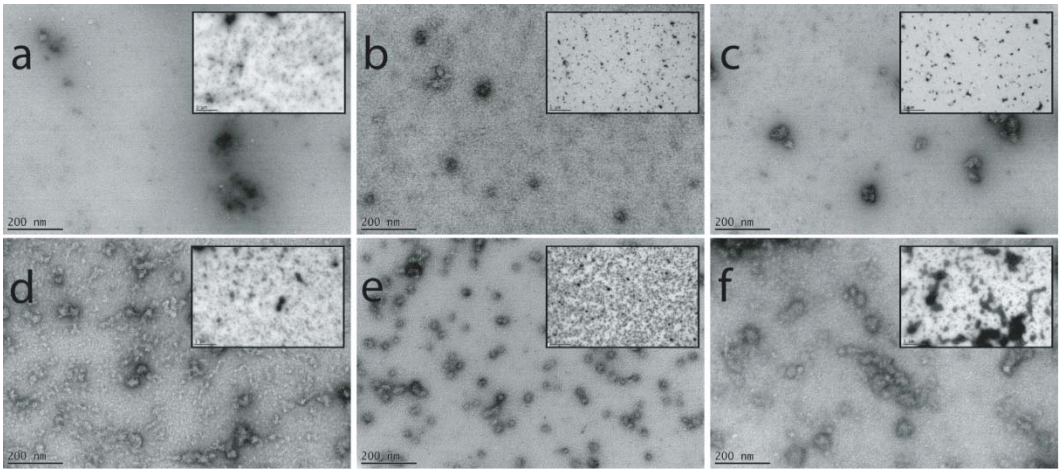

Figure 5. TEM analysis of (a) E, (b) C, (c) equal mixture of E + C, (d) EC, (e) CE and (f) ECE in which scale bar represents 200 nm. Insets represent the same proteins at 1 μm.

an average size of 34.0 ± 9.3 nm, bigger than the homopolymer sizes above; this suggested that E and C are capable of interacting (Figure 5c). The covalent block polymers appeared to exhibit a range of sizes that depend on its composition. The EC diblock yielded particles with an average size of 42.2 ± 8.0 nm, larger than the homopolymers individually and as a mixture (Figure 5d). By contrast, the CE assembled into particles that were 30.9 ± 6.7 nm, identical in size to the C homopolymer (Figure 5e). This demonstrated that the orientation of the SAD fusion and not the overall length of protein impacts the particle assembly. The ECE triblock possessed the largest particles with an average size of 50.6 ± 12.3 nm (Figure 5f). While the additional C-terminal E domain increased the particle size, the overall physical features of the EC and ECE particles were very similar while the CE characteristically looked different in shape and size. Essentially the supramolecular assembly appeared to be dictated by the orientation of the first two blocks.[9]

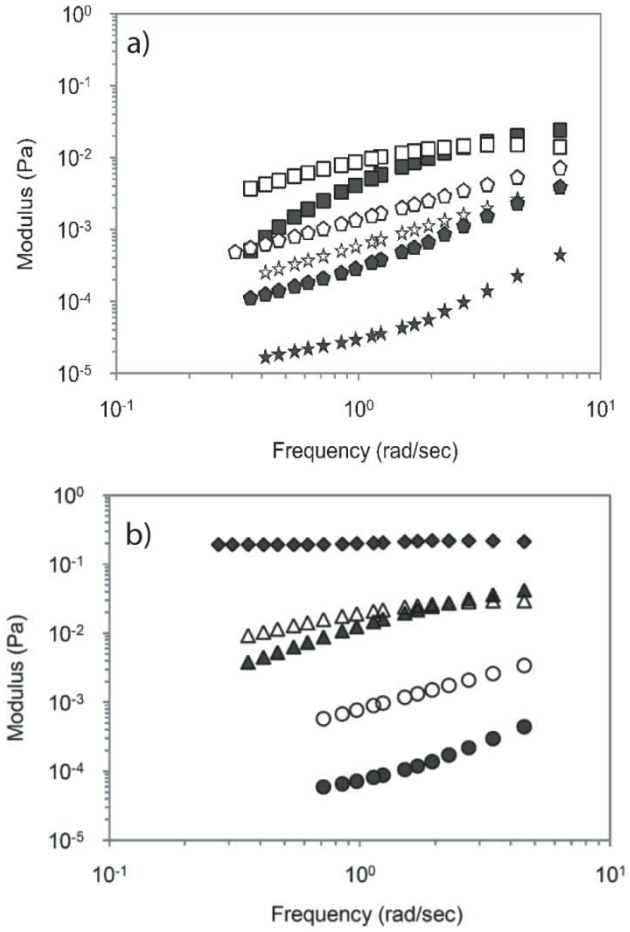

Figure 6. Microrheology of protein block polymers. Plots of G' (closed symbols) and G" (open symbols) as a function of frequency for (a) the homopolymers: E (squares), C (stars) and E+C mixture (pentagons) as well as (b) the bock polymers: EC (diamonds), CE (circles) and ECE (triangles).

To assess the bulk materials properties of the protein polymers at higher concentrations, microrheology was employed. As a control, the E and C homopolymers alone and together as a mixture were assessed. The E homopolymer was elastic at frequencies greater than 2 rad/sec while C was viscous at all frequencies examined (Figure 6a). The mixture of E+C exhibited an intermediate rheological behavior relative to each homopolymer with demonstrably more viscous character than E (Figure 6a). Remarkably, the EC diblock assembled into a hydrogel as characterized by its elastic property, while CE is completely viscous (Figure 6b). The ECE triblock posseses a viscoelastic character, sharing properties of the previous two polymers (Figure 6b). The rheological behavior of the protein bock polymers were indeed distinct from the homopolymers, indicating that the covalent conjugation of the blocks influenced the assembly and overall mechanical properties. The results corroborated our underlying hypothesis where a networked particle architecture yielded more elastic properties. The CE diblock possessed the smallest particle diameters as based on the TEM data, which led to a viscous solution under all frequencies examined. The EC diblock showed larger particles with an average diameter that appeared to be optimal for assembling into a hydrogel as demonstrated by its elastic-like mechanical properties. The addition of the C-terminal E block in the ECE triblock increased the particle size, resulting in a viscous to elastic transition at higher frequencies. While the composition of the diblocks was nearly identical, rearranging the block order from EC to CE resulted in a significant transition. Thus, the sequence orientation and block number appeared to dictate the mechanical properties.[9]

Aim 4. In order to explore the ability of the polymers to store small molecules, we investigated binding to ATR and CCM via fluorescence. Both small molecules exhibit a unique fluorescent behavior that can be readily quantified upon binding to proteins. In the case of ATR, the E homopolymer is able to bind with an increase in fluorescence by 7.7 RFU, while C binds 3.7-fold better with a significant enhancement in fluorescence (Figure 7a). The EC diblock demonstrates an increase in fluorescence by 10.3 RFU, a modest enhancement relative to E alone (Figure 7a). Interestingly, the CE diblock shows the greatest increase in fluorescence by 34 RFU, slightly more than the C homopolymer. The ECE triblock exhibits a 2.3-fold increase relative to EC but binds poorly to ATR relative to CE and C alone (Figure 7a). While the chemical structures of ATR and CCM differ, a similar trend is observed for the block polymers in the presence of CCM. The E homopolymer binds CCM with an increase in fluorescence by 17.7 RFU; C binds 2.9-fold better (Figure 7b). The EC diblock exhibits an enhancement in fluorescence by 39.7 RFU, intermediate to the E and C homopolymer data. Essentially, the CE diblock interacts strongest to CCM RFU followed by ECE and EC. Although a 2.1-fold increase in fluorescence results for ECE triblock relative to the EC diblock, a 4.5-fold enhancement is demonstrated for CE – slightly larger than what was previously observed for ATR binding (Figure 7b). In general, the presence of an N-terminal C block or the appendage of an extra E block can improve the affinity of the polymers for both compounds. All three polymers are able to interact with ATR and CCM in which the binding capacity is strongly dependent on the orientation and number of blocks. [9]

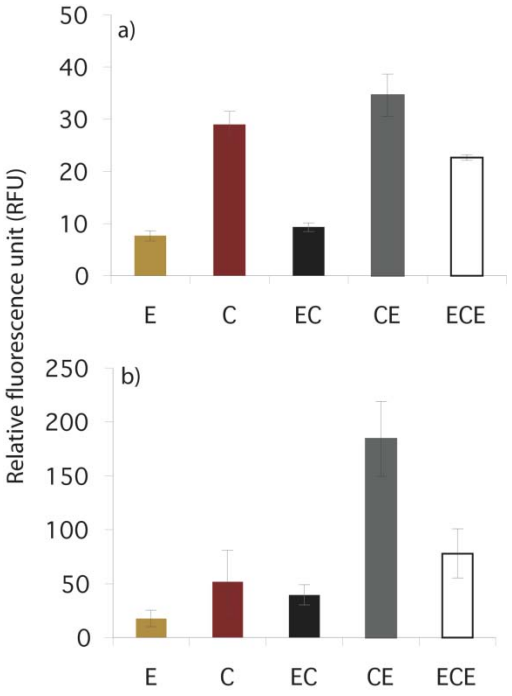

Figure 7. Fluorescence measurements of protein block polymers and homopolymers after 90 minute incubation with (a) ATR and (b) CCM.

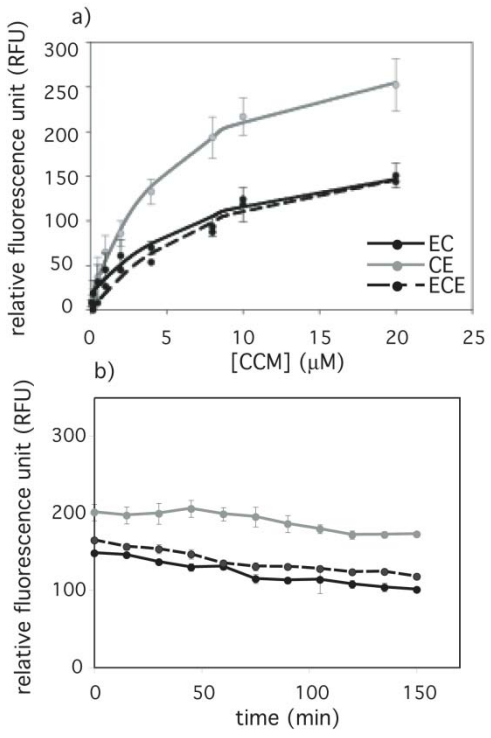

Figure 8. Plots of protein block polymers demonstrating CCM (a) binding and (b) release.

We chose to further characterize the block polymers for binding and release of CCM to assess the potential of the protein materials as vehicles for storage and delivery of small molecules. Each protein polymer under concentrations for particle formation (*vida supra)* was incubated with a range of CCM concentrations and assessed via fluorescence. From the plots of block polymer as a function of CCM, the dissociation constants (K_d) were obtained for EC, CE and ECE (Figure 8a). Of the three protein polymers, CE exhibited the best binding to CCM with a K_d of 5.7 ± 1.1 mM. Both EC and ECE revealed poorer binding relative to CE with K_d's of 9.3 ± 1.1 and 9.1 ± 0.1 mM, respectively. This confirmed that the fusion of an N-terminal C block improves the binding ability for small molecule. On the other hand, the fusion of C-terminal E block appears to make little or no difference for CCM affinity indicating that the orientation of the first two blocks is critical for binding.

Once the K_d values for CCM were calculated, the block polymers were incubated with CCM and the fluorescence intensity of the bound complex was monitored over 150 minutes. For all protein polymers, there was a loss in fluorescence indicating a release of CCM. After 150 minutes, CE was able to retain binding to CCM with 14% release followed by ECE and EC with 28% and 34% release, respectively (Figure 8b). Thus, the presence of an N-terminal C block not only improved binding to the small molecule but also resulted in slower release. Conversely, EC demonstrated the fastest release and appending an additional E block retards the CCM release. In contrast to the binding studies above where the first two blocks dictate CCM affinity, the orientation and number of blocks contribute to the release profile.

Aim 5. Our previous studies on the mechanical properties of the block polymers demonstrated that the depending on the orientation of the blocks, the polymers are elastic or viscous (Figure 6). In order to assess at what concentration do the mechanical properties of the EC and CE block polymers change, we performed a serial dilution and measured the rheological properties at the various concentrations.

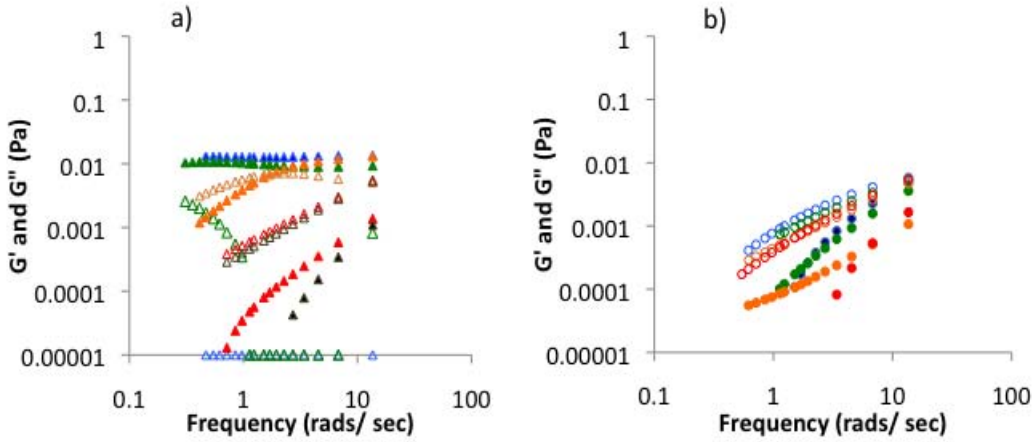

Figure 9. Microrheology of (a) EC and (B) CE as a function of concentration. Plots of G' (closed symbols) and G" (open symbols) as a function of frequency. Blue=10 mg/mL, green=5mg/mL, orange=2.5 mg/mL, red=1.25 mg/mL and black=0.625 mg/mL.

Based on the microrheology, EC maintains a predominantly elastic structure at a high concentration range up until 2.5 mg/mL, which results in viscoelastic character (Figure 9a). At concentrations of 1.25 mg/mL EC become essentially viscous (Figure 9b). Thus, there is a threshold concentration of EC, which is needed in order to form networks and gel-like structure. In the case of CE, the materials are viscous under all the concentrations.

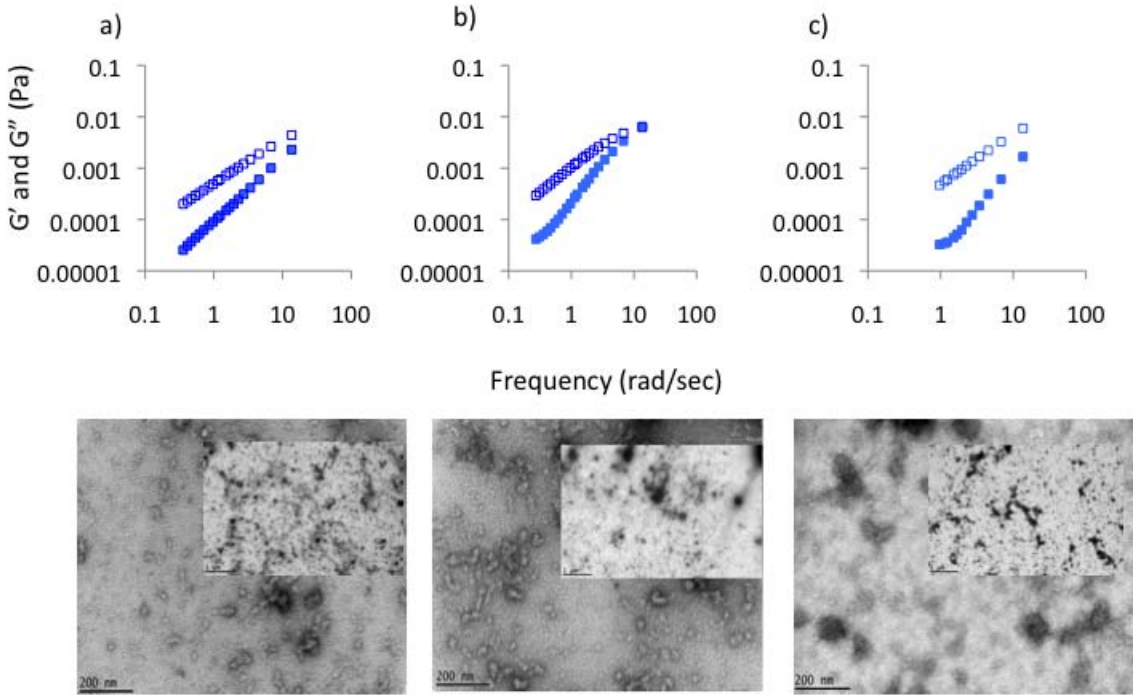

Figure 10. Microrheology and TEM analysis of (a) CE:ECE, (b) CE:EC and (c) EC:ECE. Plots of G' (closed symbols) and G" (open symbols) as a function of frequency. Scale bars represent 200 nm and insets show scale bars of 1μm.

With an understanding of the physicochemical properties of each block polymer, we generated 1:1 mixtures of CE:ECE, CE:EC and EC:ECE and performed microrheology as well as TEM analysis (Figure 10). All mixtures demonstrate viscous character. As demonstrated above, the block polymers alone exhibited distinct mechanical properties however, the mixtures revealed different overall character that cannot be attributed to an equal mixture of each component. The viscoelastic behavior observed with the CE:ECE mixture could potentially be due to ECE and the viscous property of the EC:CE could be due to CE. However, in the EC:ECE mixture, neither block polymer alone possessed the overall viscous character. This indicated that within the mixture, each of the components interacted with one another to provide the final measured property. To assess what types of structures the combined polymer mixtures would form, we performed TEM. All the mixtures revealed a range of particles with different shapes. The CE:ECE mixture presented the largest particles size of 35 .6 ± 11.4 nm followed by CE:EC which exhibited particle sizes of 32.9 ± 10.1 nm. Interestingly, EC:ECE demonstrated the smallest particles sizes of 15.6 ± 4.1 nm. These particles observed in the mixtures were

different from the particles of each block polymer alone (Figure 5), confirming the interactions of each component in the mixture. This work is being written up for publication.

Aim 6. The 10 residues in the ***a*** and ***d*** positions lining the pore of COMPcc^s (C) were individually mutated into alanine via site-directed mutagenesis (Figure 12).[10] Each alanine variant in addition to the wt was characterized for structure, stability and oligomerization state. Binding of the variants to the hydrophobic small molecules vit D, ATR and ccm were also assessed.

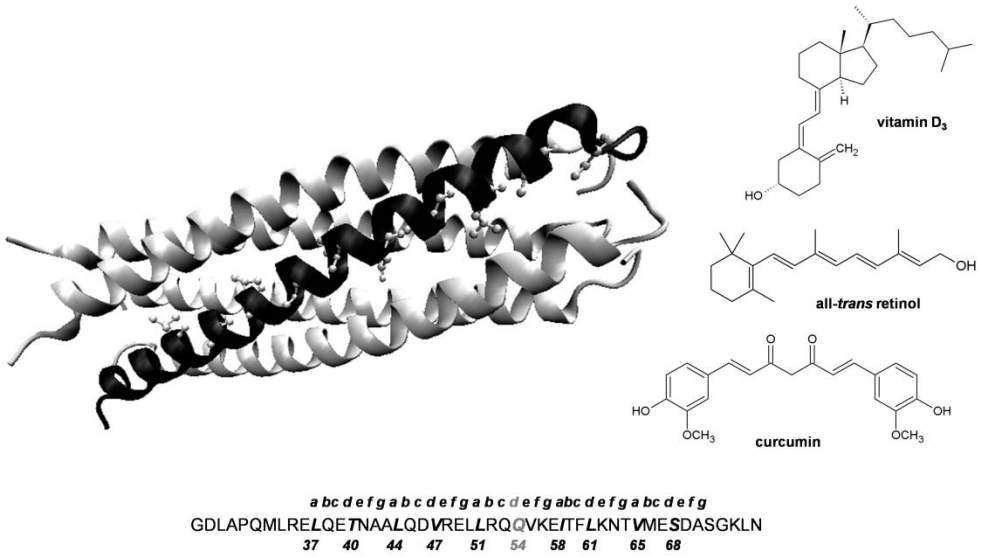

Figure 12. Structure and sequence of COMPcc^s in which the residues mutated into alanine are represented in bold italics where Q54, which divides the pore into two pockets is highlighted in grey (left). The chemical structures of the small molecules 1,25-dihydroxyvitamin D_3, all-*trans* retinol and curcumin are shown (right).

Impact of variants on α-helicity. Far UV circular dichroism (CD) was employed to determine the secondary structure of wt and variants at room temperature. Wavelength scan of wt demonstrated a double minima at 208 and 222 nm indicative of an α-helix with a calculated fractional helicity of 70.1% as previously reported (Figure 13a). Variants L37A, L44A, V47A, L51A, I58A exhibited a substantial loss in α-helical structure (Figure 13a). Each of these variants expressed a fractional helicity with less than 50% and a $\Theta_{222}/\Theta_{208}<1$, indicating that these residues are critical for the maintenance of α-helix. Variants L61A, V65A and S68A showed a modest decrease or no change in helical content (Figure 13a). These variants possessed a 58%-69% fractional helicity and retained a $\Theta_{222}/\Theta_{208} \geq 1$. Finally, the two variants T40A and Q54A illustrated an increase in α-helicity as demonstrated by the >80% fractional helicity values and $\Theta_{222}/\Theta_{208}>1$.

Of the total residues that line the first pocket divided by Q54, all the aliphatic residues L37, L44, V47 and L51 appear to play a significant role in maintaining the helix (Figure 12). Residue I58 is the only residue located within the second C-terminal pocket that

yielded a significant loss in helical content when mutated into alanine. The remaining residues L61, V65 and S68 within the second pocket bear modest implications on the α-helix. The two polar residues, T40 and Q54, improve the helical content when mutated into alanines in the first pocket. Together this suggests that the residues within the N-terminal pocket are important in establishing and maintaining the helical structure, while the C-terminal residues do not substantially influence the α-helix.

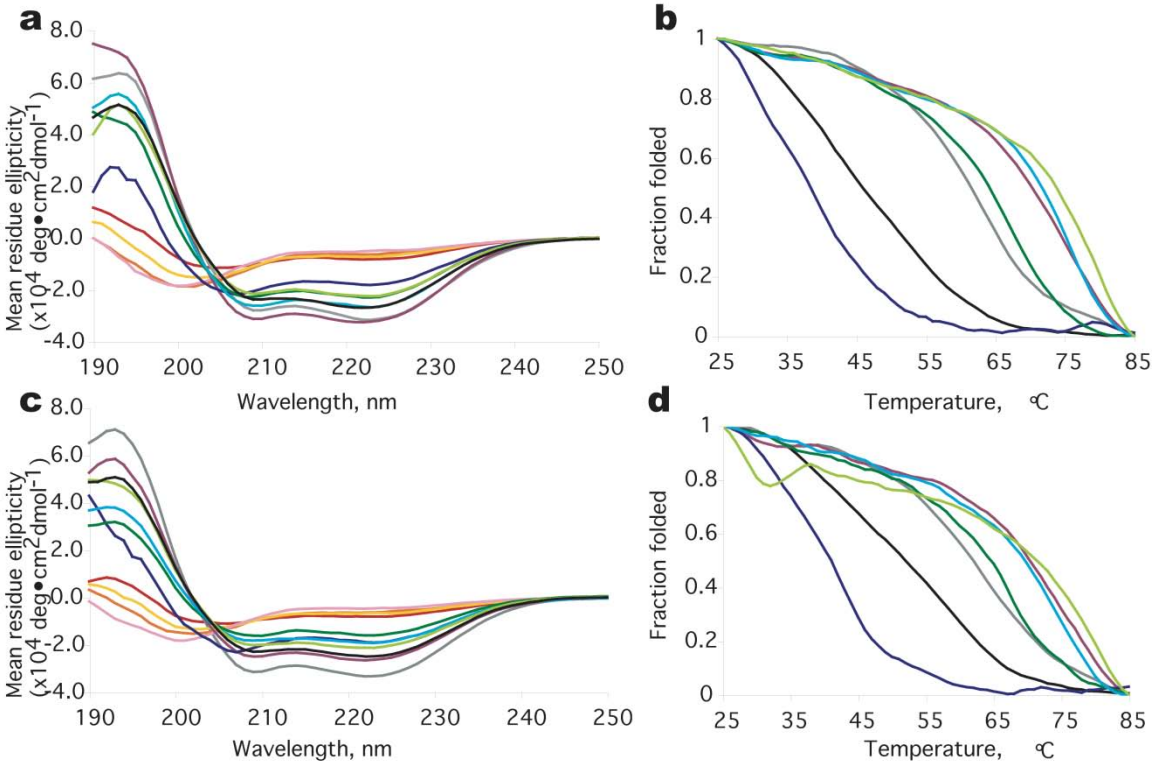

Figure 13. CD spectra of COMPcc^s and single alanine variants in the absence (**a**, **b**) and presence (**c**, **d**) of vit D. (**a**, **c**) Wavelength scans at room temperature (25^{o}C) and (**b**, **d**) temperature scans at 222 nm of COMPcc^s (black), L37A (red), T40A (grey), L44A (orange), V47A (yellow), L51A (pink), Q54A (purple), I58A (blue), L61A (green), V65A (light blue), and S68A (light green). All scans represent an average of 2 trials.

Impact of variants on thermostability. Temperature scans at 222 nm were performed to determine the thermostabilities of all the proteins. The wt presented a cooperative thermal transition temperature (T_m) of 44.7^{o}C, similar to previously reported values. Of the six variants that produced a discernable melting curve, five demonstrated a significant increase in thermostability relative to wt. Variant V65A displayed a 41.5^{o}C enhancement in T_m, the largest increase observed from all the variants. This was followed by Q54A and S68A, which showed a 35.6 and 32.3^{o}C improvement, while variants L61A and T40A presented a 20.6 and 16.4^{o}C increase relative to wt. By contrast, variant I58A displayed an 8.5^{o}C decrease in T_m, when compared to wt.

The reversibility and monophasic behavior of the melts enables us to assume a 2-state mechanism of unfolding. As a result, we can calculate the thermodynamic parameters of the aforementioned variants and wt based on the fraction folded**.** The stability of wt COMPcc arises from a strong enthalpic component with a Van't Hoff enthalpy (ΔH) of –

35.2 kcal•mol^{-1} (Table 1). This leads to a calculated Gibbs free energy (ΔG) of –2.4 kcal•mol^{-1}. In general, for the T40A and Q54A variants that exhibited enhanced helical content and stability, an increase in free energy of 1.8 and 2.0 kcal•mol^{-1} is observed relative to wt, respectively (Table 1). The remaining C-terminal residues L61, V65 and S68 demonstrated a 2.9, 2.2 and 1.1 kcal•mol^{-1} increase in stability respectively

Table 1: Summary of the calculated thermodynamic parameters

Protein	-Vitamin D			+Vitamin D		
	ΔH^{o}[a] (kcal•mol^{-1})	ΔS^{o}[b] (kcal•mol^{-1}•K^{-1})	ΔG^{o}[c] (kcal•mol^{-1})	ΔH^{o}[a] (kcal•mol^{-1})	ΔS^{o}[b] (kcal•mol^{-1}•K^{-1})	ΔG^{o}[c] (kcal•mol^{-1})
COMPcc[s]	-85.2	-0.27	-4.3	-64.7	-0.20	-4.0
T40A	-115.3	-0.34	-12.7	-104.1	-0.30	-11.7
Q54A	-125.9	-0.36	-17.7	-129.6	-0.37	-19.2
I58A	-109.98	-0.35	-4.5	-133.6	-0.42	-6.7
L61A	-127.7	-0.37	-15.6	-146.8	-0.43	-18.1
V65A	-162.4	-0.46	-23.7	-130.2	-0.37	-18.7
S68A	-173.3	-0.49	-27	-144.9	-0.40	-22.9

[a] Van't Hoff enthalpy calculated as described in Experimental Procedures
[b] At equilibrium, $\Delta G^{o} = 0$. Hence, the change in entropy (ΔS^{o}) = $\Delta H^{o}/T_m$
[c] Free energy of folding at 25 °C calculated by the expression, $\Delta G^{o} = \Delta H^{o} - T\Delta S^{o}$

compared to wt when substituted to alanine (Table 1). By contrast, I58A revealed a 0.8 kcal•mol^{-1} loss in stability relative to wt (Table 1).

The majority of the residues that impact the thermostability are located within the second pocket starting from the division point of Q54 (Figure 1). C-terminal residues L61, V65 and S68 stabilize the protein when mutated into alanine, while alanine at position 58 destabilizes it. This demonstrates the significance of I58 in maintaining stability. Although most of residues that influence stability are localized on the C-terminal end, T40 and Q54 within the first pocket also affect the thermostability when converted into alanine. The enhancement in stability observed by these two variants appears to be linked to the improved helical content described above.

Impact of variants on oligomerization state. In order to determine the oligomerization states of wt and variants, crosslinking studies were performed using bis(sulfosuccinimidyl)-suberate (BS^3) under the same concentrations used for CD and analyzed on SDS-PAGE. The wt COMPcc demonstrated the presence of five equally intense bands indicating the presence of pentamers, in addition to tetra-, tri-, di- and monomers (Figure 14). In contrast, variants L37A, L44A, V47A and L51A exhibited predominantly monomer bands. Both L44A and L51A showed evidence for dimer in addition to the monomer. V47A displayed the existence of di-, tri- and tetramers, while L37A demonstrated the presence of di-, tri-, tetra- and pentamers with less intensity than the monomer band. Variants T40A, Q54A, I58A, L61A, V65A and S68A illustrated an

enhanced oligomerization in which the monomer band disappeared, while retaining the di-, tri- tetra- and pentamer bands (Figure 14).

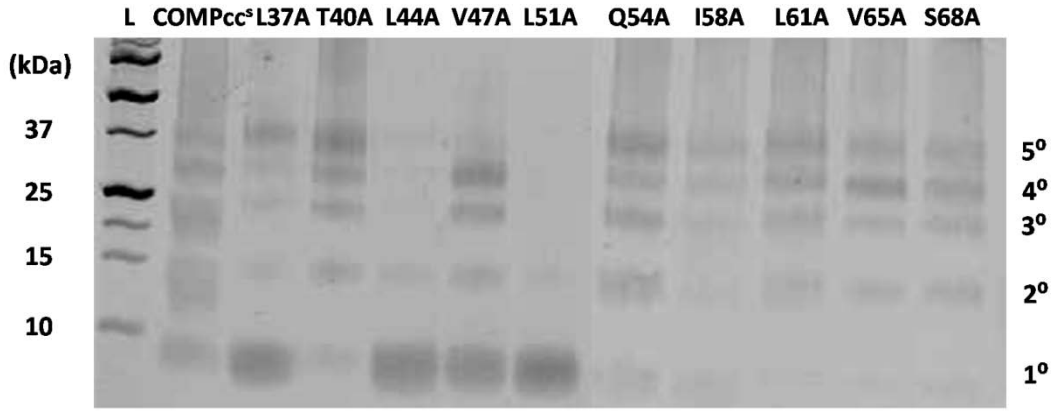

Figure 14. SDS-PAGE of crosslinking of variants by bis[sulfosuccinimidyl] suberate (BS^3). L Protein marker. The crosslinked samples were run on a 12% SDS-PAGE to determine the oligomerization state of the variants. The molecular weights are indicated on the left and the mono- (1^o), di-,(2^o) tri- (3^o), tetra- (4^o) and (5^o) pentamer populations are indicated on the right.

In general, the residues L37, L44, V47 and L51 important for maintaining the oligomeric state of the protein are positioned in the N-terminal pocket region since mutation into alanine abolishes the presence of the pentamer bands. However, residues T40, Q54, I58, L61, V65 and S68 do not appear to be critical for pentamerization. In fact, mutation into alanine facilitates oligomerization. These residues are mostly distributed at the C-terminal end with the exception of two polar residues, T40 and Q54 that reside in the N-terminal region.

Influence of vitamin D. One of the key features of COMPcc is its ability to bind vit D as demonstrated by structural and biochemical studies.[5] Vit D is an important hormone involved in promoting cellular differentiation and proliferation in terms of cartilage and bone tissue in addition to the maintaining of calcium and phosphate homeostasis.[11,12] To investigate the impact of the presence of vit D on COMPcc, we performed CD and crosslinking studies after incubating wt and variants with the small molecule.

The proteins before and after binding vit D were compared to evaluate whether there is any effect of vit D on helicity. Variants L37A, L44A, V47A, L51A, I58A, L61A, V65A and S68A exhibiting large and modest losses in α-helical content revealed similar decreases, while those variants T40A and Q54A demonstrating enhanced helicity maintained an increase with respect to wt COMPcc in the presence of vit D (Figure 13). Nearly all the variants including wt showed a slight loss in helical content upon incubation with vit D relative to the unbound proteins, except T40A and I58A.

As described for the variants in the absence of vit D, similar increases and decreases were observed in T_m relative to wt COMPcc (Figure 13). Variants Q54A, V65A, S68A, L61A and T40A presented an increase in T_m ranging from 28.8 to 11.4^{o}C, while I58A showed

decrease by 11.3 ^{o}C when compared to wt. Previously, COMPcc binding to vit D was detected by a shift in the T_m. The wt demonstrated an increase in the T_m of 6.2^{o}C upon incubation with vit D, affirming earlier data (Figure 13). Variant I58A exhibited a 3.4^{o}C increase, followed by Q54A, T40A and L61A, which revealed a 1.8, 1.4 and 0.7^{o}C enhancement, respectively indicating decreased binding relative to wt. However, variant S68A did not affect the T_m while V65A illustrated a decrease in T_m by 6.5^{o}C (Figure 13). The variants L37A, L44A, V47A an L51A were unable to bind vit D due to their inability to form α-helices.

To study the impact of vit D on oligomerization, crosslinking studies were performed after incubation with vit D. A similar trend was observed in which L37A, L44A, V47A and L61A demonstrated mostly monomers or lack of pentamer formation while the remaining T40A, Q54A, I58A, L61A, V65A and S68A exhibited strong pentamer bands.

Binding to all-trans retinol and curcumin. Variants L37A, L44A, V47A, L51A, I58A and L61A demonstrated dramatic losses in binding indicating that these residues may be critical for ATR recognition (Figure 15a). The N-terminal residues L37, L44, V47 and L51 responsible for the maintenance of helical content and oligomerization state bound poorly to ATR when substituted to alanine. By contrast, the variant Q54A that previously illustrated enhanced helical content and oligomerization, revealed an increase in fluorescence, indicative of improved binding. Interestingly, S68A previously shown to display modest effects on the coiled-coil structure and self-assembly also bound slightly better to ATR.

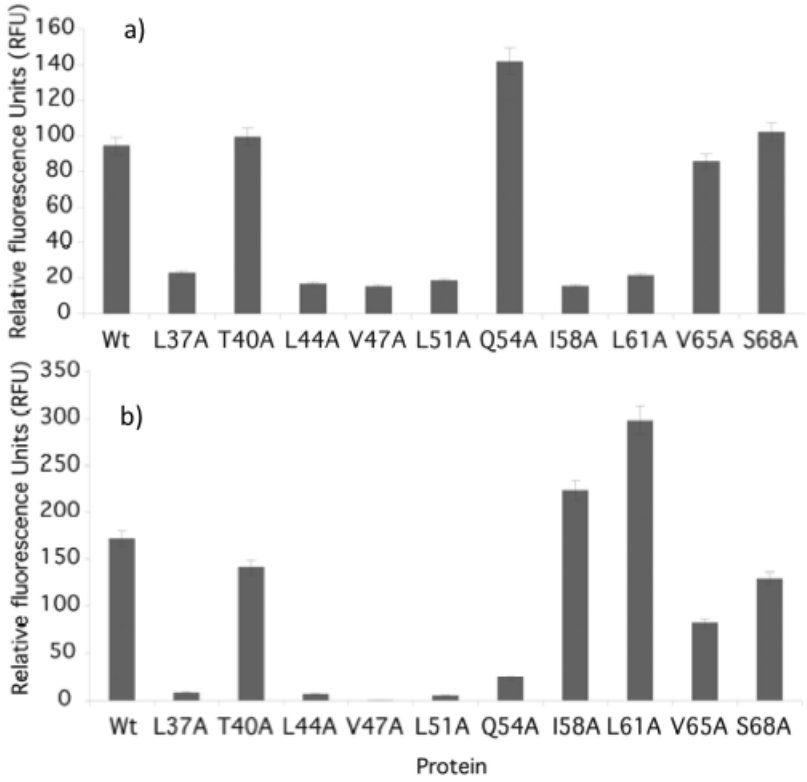

Figure 15. (a) ATR and (b) CCM fluorescence binding studies of COMPcc^{s} and variants.

Variants, L37A, L44A, V47A, L51A and Q54A demonstrated significant reduction in binding (Figure 15b). The four residues L37, L44, V47 and L51 positioned in the N-terminal pocket were previously noted to be essential for helicity and oligomerization also bound ccm poorly when substituted with alanine similar to the ATR studies. Notably, I58A and L61A revealed an increase in fluorescence relative to wt COMPcc (Figure 15b). Comparison of ATR and ccm binding studies reveal a consistency in the binding abilities of the variants for both substrates, however, variants Q54A, I58A and L61A demonstrate a clear preference either ATR or ccm. These results suggest that the residues that line the pocket play an important role in selectively binding various hydrophobic small molecules.

Interplay of helicity, stability and oligomerization. Residues L37, L44, V47 and L51 that exhibited a substantial loss in helicity when substituted by alanine were not sufficiently stable to determine melts, while I58A which showed modest loss in α-helical structure demonstrated a loss in T_m. These results suggest that the residues critical for maintaining helical content are important for preserving the stability. Moreoever, the residues L37, L44, V47 and L51 that no longer displayed helical structure and discernable stability when mutated into alanine revealed predominantly monomeric states (Figures 13, 14).

The residues important for structure, stability and pentamer formation are located in the N-terminal pocket. Based on the heptad pattern, L37, L44 and L51 occupy the ***a*** position while V47 occupies the ***d*** position (Figure 12). Thus, the stability of the pentameric assembly is largely mediated by the interactions between three leucines from one helix with a valine from the adjacent helix. Another pentameric coiled-coil, phospholamban, has been demonstrated to be governed by the packing interactions between three N-terminal leucines, L37, L44 and L51, in the ***a*** position with two isoleucines, I40 and I47, in the ***d*** position from a neighboring helix.[13] This suggests that an N-terminal repeat of 3 leucines in the ***a*** site along with a valine or set of isoleucines in the ***d*** site of the adjacent helix are indispensible for the formation of pentamers.

The two polar residues, T40 and Q54 that improved the α-helical content when mutated into alanine also demonstrated a substantial increase in T_m. Alanine substitution of either residue in this N-terminal region resulted in pentamer formation and enhanced oligomerization (Figures 14, 15). In this case, increased helicity and stability facilitates the oligomer formation.

The remainder of the residues L61, V65 and S68 located in the C-terminal region when substituted with alanine yielded a modest loss in helical content (within 15%), while exhibiting an enhanced stability. Interestingly, alanine substitution of these residues maintains the pentamer formation and improves the oligomerization state where the monomer population essentially disappears (Figures 14, 15). Here, the C-terminal residues maintain the link between stability and oligomerization as long as a threshold level of α-helical structure is maintained.

Influence of vit D on helicity, stability and oligomerization. No significant change in

helical content, stability and oligomerization was observed in the presence of vit D for the COMPcc^s and alanine variants relative to the unincubated proteins. The major discernable differences can be identified from shifts in the T_m. Variants T40A, Q54A, I58A, L61A and S68A in addition to COMPcc^s exhibited an increase or no change in the T_m, indicating binding of vit D. These five span both pockets with a majority concentrated in the C-terminus and do not play a significant role in the vit D recognition. The variant V65A exhibits a decrease in T_m, suggesting that it may be important for vit D binding. However, residues L37, L44, V47 and L51 represent the most crucial in vit D recognition as absolutely no binding can even occur due to the inability to oligomerize as described above.

Variants that exhibit specific preference for vit D, ATR or CCM. From the vit D, ATR and CCM studies, variants Q54A, I58A and L61A demonstrated selective binding. Variant Q54A exhibited enhanced affinity for ATR while illustrating poor binding to CCM and vit D (Figures 13d, 15). Remarkably, two variants I58A an L61A bound specifically to CCM, while weakly binding ATR and vit D (Figures 13d, 15). Thus by altering the sequence within the binding pocket, it may be possible to control the specificity for small molecule binding.

Aim 7. Employing the C homopolymer and variants thereof from the previous aim, we explore the effect of divalent metals on the folding and assembly. Since the homopolymer constructs are generated with an N-terminal hexa-His tag, we anticipate that it can bind to divalent metal ions Zn (II) and Ni (II). While it is unknown what the effects of the metal binding has on the structure of the hexa-His tag, here we investigate how Zn (II) and Ni (II) influences the overall conformation of C, T40A (a highly stable, helical C variant) and L44A (a destabilized, random conformation C variant).

To assess both secondary structure and thermal stability of all three proteins in the absence and presence of Zn(II) and Ni(II), we performed CD (Figure 16, Table 2). The C homopolymer possessed distinctive double minima at 208 and 222 nm indicative of an α-helix with a calculated helical content of 55%. By monitoring the signal at Θ_{222} as a function of temperature, the thermal melting transition (T_m) was calculated to be 48 °C, consistent with values obtained from the previous aim (Figure 16a, Table 2).[10] In the presence of 100 μM of Zn(II), the helical content of the protein increased to 63% along with a drastic increase

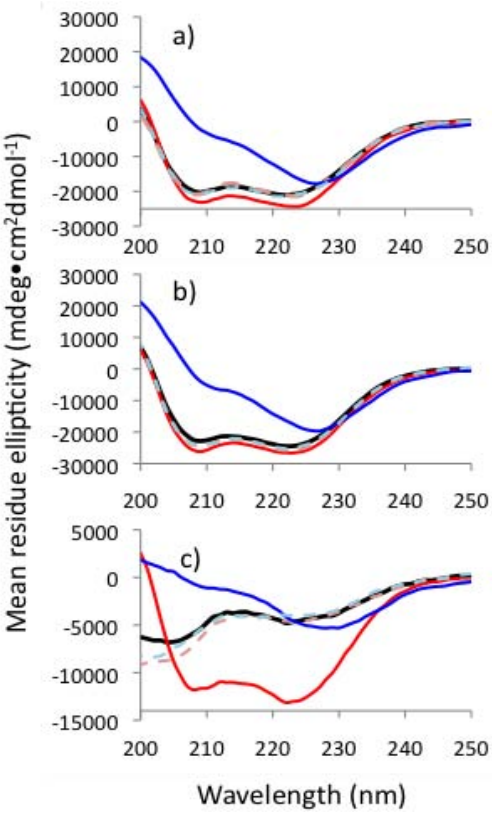

Figure 16. CD of (a) C, (b) T40A and (c) L44A in the absence (black) and presence of Ni(II) (blue), Ni(II)+EDTA (light blue), Zn(II) (red) and Zn(II)+EDTA (pink).

in stability (T_m greater than 80 °C) (Figure 16a, Table 2). By contrast, a large loss in the minimum at 208 nm in addition to a red shift in the minimum from 222 nm to 225 nm was observed in the presence of 100 μM of Ni(II) (Figure 16a, Table 2). This phenomenon was indicative of higher order aggregate formation and particulate systems. At higher concentrations of protein (100 μM), binding of Ni(II) resulted in the formation of insoluble precipitate due to aggregation (data not shown). While an overall loss in helical content to 38% was observed, there was a 15 °C increase in T_m (Figure 16a, Table 2). Ethylenediaminetetraacetic acid (EDTA) was added to the bound structure to sequester the metals. Upon chelation of Zn(II) and Ni(II) with 1 mM of EDTA, the spectra resembled its original characteristics with similar helical content and thermal mid-point of transitions (Figure 16a, Table 2).

In the case of the stable variant, T40A, a more negative double minima was observed with a corresponding total helical content of 69% and a melting temperature of 62°C, similar to the values reported earlier (Figure 16b, Table 2). Addition of 100 μM of Zn(II) increased the T_m beyond 80°C while the helical content was raised by 5%. A similar loss in the minima at 208 nm was observed upon Ni(II) (100 μM) binding leading to a loss in helical content to 45%. The minima at 222 nm slightly red-shifted to 224-225 nm. Aggregation was observed in the form of insoluble precipitate. Despite the reduction in helical content, a 6°C increase T_m was observed. Addition of 1mM EDTA to both the Zn (II) and Ni(II) complex with T40A lead to reversion to its original structural and thermal properties.

Table 2. Summary CD data in the presence and absence of divalent metals and EDTA

Protein	$-\Theta_{208}$ (deg cm^2 dmol^{-1})	$-\Theta_{222}$ (deg cm^2 dmol^{-1})	% Helicity	T_m (°C)
His-C	19729	21208	55	48
His-C + Zn	22997	24289	63	>80
His-C+ Ni	963	14836	38	63
His-C + Zn + EDTA	20522	21412	55	48
His-C + Ni + EDTA	21021	21802	56	50
His-T40A	24793	26719	69	62
His-T40A + Zn	27476	28433	74	>80
His-T40A + Ni	3413	17568	45	68
His-T40A + Zn + EDTA	26296	27705	72	62
His-T40A + Ni + EDTA	25964	27303	71	61
His-L44A	6971	5099	13	-
His-L44A + Zn	14521	15633	40	72
His-L44A + Ni	566	6602	17	58
His-L44A + Zn + EDTA	7996	5114	13	-
His-L44A + Ni + EDTA	7788	4919	12	-

In the absence of divalent metals, L44A revealed a random coil conformation with a single minimum around 201 nm as expected (from the previous aim). This variant exhibited a low helical content of 13% and thus did not exhibit a measurable T_m (Figure 16c, Table 2). Remarkably, addition of Zn(II) changed the conformation of the protein from random coil to α-helix. There was an increase in helical content to 40%; more importantly, a T_m of 72°C was observed. The L44A•Zn(II) complex demonstrated reversible structure and thermal denaturation curves, indicating that the path of Zn(II)-

assisted refolding is energetically favorable than the path by which the peptide alone is refolding (data not shown). The presence of Ni (II) yielded a similar effect on L44A where a loss in 208 nm minima as well as a red shift of the 222 nm minima was observed. Although the helical content was 17%, there was a considerable increase in the thermal stability of the protein (58°C) (Figure 16c, Table 2). Unlike the case of Zn(II), the L44A•Ni(II) complex did not demonstrate a reversible structure and thermal denaturation curves (data not shown). In the presence of EDTA, the spectra resumed random coil conformation and a loss in T_m. The Zn(II) and Ni(II) exhibited a differential binding pattern (with structural and thermostability consequence) for all the proteins investigated.

The ability to bind CCM was assessed for all proteins at 10 μM in the absence and presence of 100 μM metals. In the absence of metals, C and T40A exhibited binding to CCM while L44A was unable to bind, confirming our earlier studies (Figure 17). In the presence of Ni (II), a loss in binding by approximately 5 fold was observed for both C and T40A, while L44A showed an 18 fold increase in fluorescence relative to the L44A alone, indicating CCM binding. The loss in binding can be attributed to the loss in helical structure observed upon incubation with Ni (II) for C and T40A (Figure 16). The addition of Zn (II) resulted in CCM recognition for both C and T40A with nearly identical RFU values as the proteins in the absence of metals. Remarkably, L44A in the presence of Zn (II) showed a 111 fold increase in binding ability for CCM relative to the protein alone (Figure 17). This change could be attributed to formation of helical structure of L44A in the presence of Zn (II) (Figure 17).

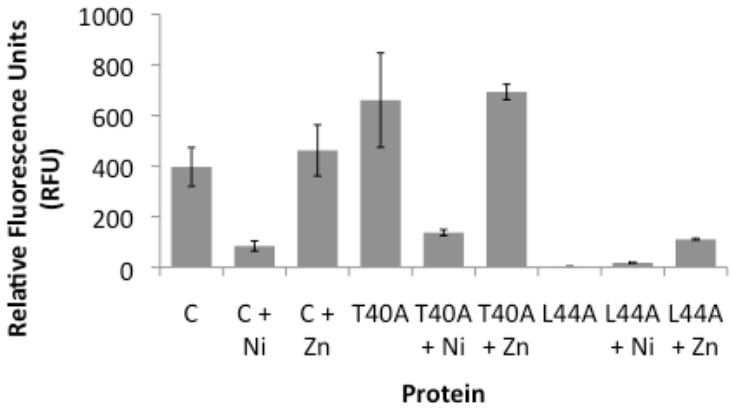

Figure 17. Fluorescence of CCM bound to protein in the absence and presence of metals.

The supramolecular assemblies of the homopolymers in the absence and presence of Ni (II) or Zn (II) were assessed via TEM after incubation for one day. Both C and T40A exhibited the formation of fibers at 10 μM, while L44A did not show any discernable formation of fibers (Figure 18). The resulting fibers possessed diameters of 7-7.5 nm, which represented the length of the helical coiled coil. Upon addition of Ni (II), higher order aggregates of fibers appeared to form for both C and T40A, while particle aggregation was observed for L44A. In the presence of Zn (II), both C and T40A revealed fibers that were shorter than the fibers in the presence of Ni (II); C appeared to have twisted groups of fibers that have double the diameters of 14 nm while T40A showed fibers that were untwisted (also with diameter of 14 nm. By contrast, L44A in the presence of Ni (II) showed no significant change relative to the particles observed in

the absence of any metal. Based on the prior secondary structure analysis, fiber formation depended on the ability of the proteins to assemble into helices as both C and T40A produced fibers while L44A did not as it was unstructured.

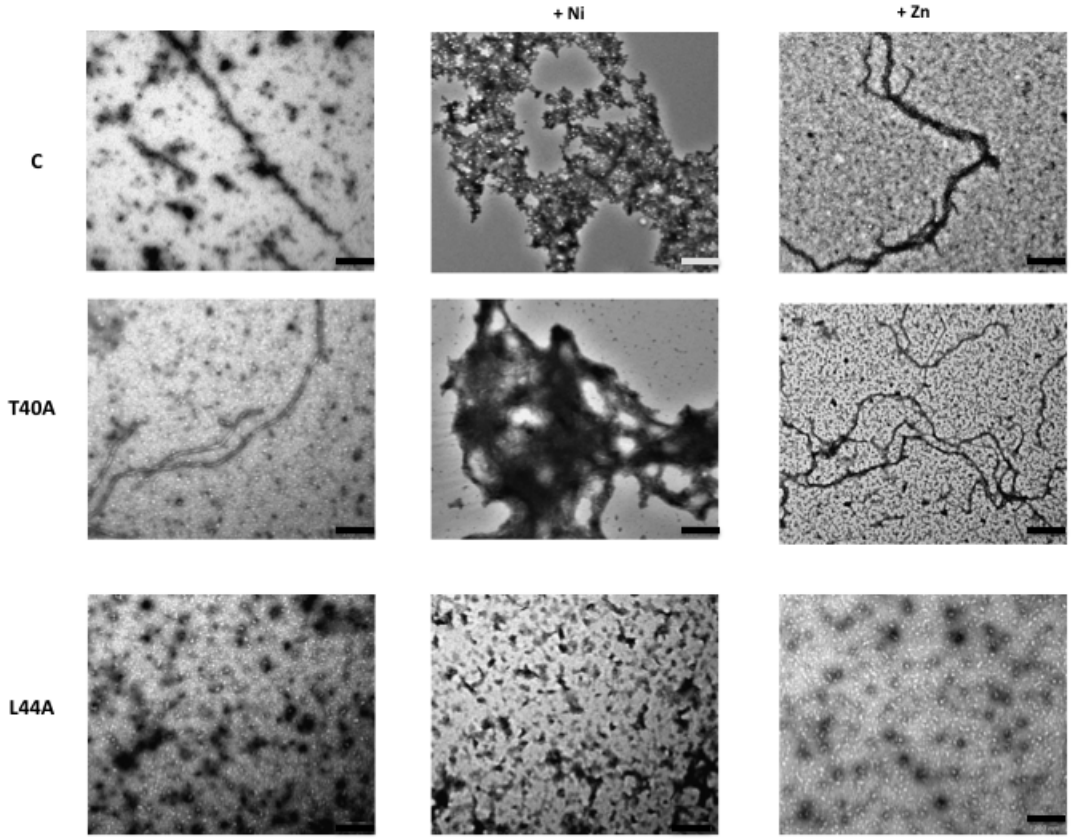

Figure 18. TEM of C, T40A and L44A in the absence and presence of Zn (II) or Ni (II). Black scale bars represent 200 nm while grey scale bar represents 1 μm.

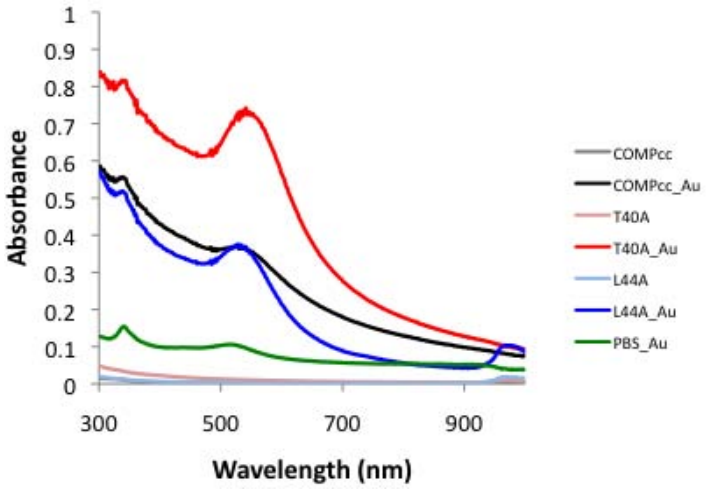

Figure 19. Absorbance scan of C, T40A and L44A in the absence and presence of gold.

In addition to metal dependent assembly, we explored the ability of the same proteins to template the formation of gold particles. Proteins at a concentration of 10 μM were incubated in the presence of 5 mg of trimethylphosphinchlorogold salt and reacted overnight in the dark at room temperature. The excess salt was removed by centrifugation and the gold bound protein were reduced by addition of hydrazine hydrate

and incubated overnight in the dark at room temperature. Formation gold particles were confirmed via absorbance by the presence of a characteristic plasmon resonance peak at 520 nm. While both C and L44A appeared to have similar absorbance peaks, T40A demonstrated a > 2 fold increase in absorbance. Since it appeared to exhibit the largest plasmon resonance peak, we performed TEM analysis of T40A in the absence and presence if gold. The TEM data showed that indeed gold nanoparticles were generated *in situ*. Moreover, the gold nanoparticles appeared to line the edges of the T40A fiber (Figure 20). This work is being written up for publication.

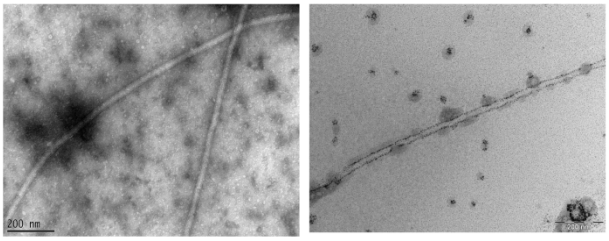

Figure 20. TEM images of T40 in the absence (left) and presence (right) of Au. Scale bars represent 200 nm

Aim 8. With the complete characterization of the block polymers mentioned above, we explored the length dependence of the E block on the EC and CE diblock polymers. A library of E_mC and CE_m was fabricated in which the E domain was systematically truncated. This would enable control of the thermoresponsive behavior so that we can tune the transition temperature. Essentially, 8 library members were biosynthesized and characterized for secondary structure, stability (T_m) and inverse temperature transition (T_t).

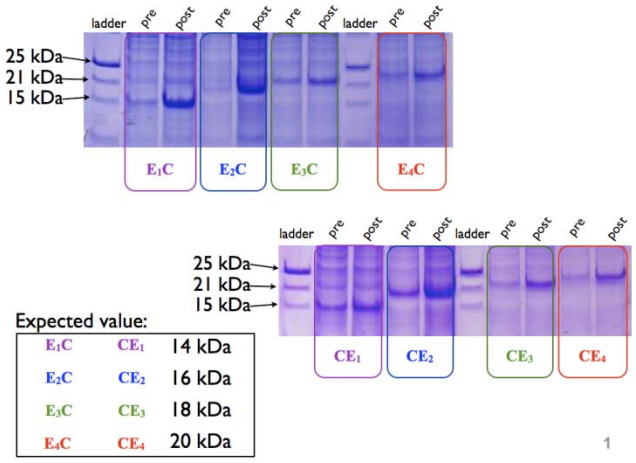

Figure 21. SDS PAGE of E_nC and CE_n protein library expressions.

By modifying the PCR amplification conditions, we were able to isolate systematically truncated lengths of elastin DNA using a single template pUC19ELP pentamer (gift from D. Tirrell). The resulting elastin fragments were restricted and cloned N- or C-terminally to the COMPcc gene, leading to a total of 8 possible E_nC and CE_n diblock library members. The constructs were transformed into *E. coli* BL21DE cells and expressed (Figure 21). A single colony of each construct was picked and grown overnight at 37°C. Luria broth (LB) containing ampicillin (200 mg/mL) was inoculated with an overnight culture. After the culture was grown to an OD_{600} of 1.0, protein expression was induced by adding isopropyl-beta-D-thiogalactopyranoside (IPTG) to a final concentration of 1 mM and incubated at 37°C. Cells were harvested after 3 hours by centrifugation at 6000 rpm at 4°C and stored at –

80°C. SDS PAGE was performed on whole cell lysates of pre- and postinduction samples (Figure 21).

The pellets were resuspended in lysis buffer containing 100 mM NaH_2PO_4, 10 mM Tris Cl, 8 M Urea pH, 8.0 and subjected to two cycles of freeze thawing. Whole cell lysates were clarified and subjected to purification by Ni-NTA columns according to the manufactured protocol under denaturing conditions (Qiagen: Valencia, CA). The level of purity for each protein was monitored by PAGE analysis and verified by MALDI mass spectrometry. Concentrations of purified proteins were measured by Bradford protein assay (BioRad: Hercules, CA) with bovine serum albumin (BSA) as a standard. Proteins were dialyzed in 10 mM phosphate buffer pH 8.0 to remove denaturants and further characterized.

Characterization of E_nC and CE_n library constructs via CD. To gain a better understanding of the structure and stability of the purified E_nC and CE_n diblock library members from above, circular dichroism (CD) experiments were performed [14]. The dialyzed proteins were scanned on a Jasco J-815 CD spectrophotometer equipped with a PTC-423S single position Peltier temperature control system and counter-cooled with an Isotemp 3016S water bath using 0.1 cm optical path Hellma 218 quartz cuvette.

A far-UV temperature-dependent wavelength scan from 190-250 nm was completed for E_1C, E_2C, E_3C, E_4C, CE_1, CE_2, CE_3, and CE_4 (Figure 22). In order to maintain soluble protein polymer under high temperatures, 0.33 M GuaHCl was added to the buffer when

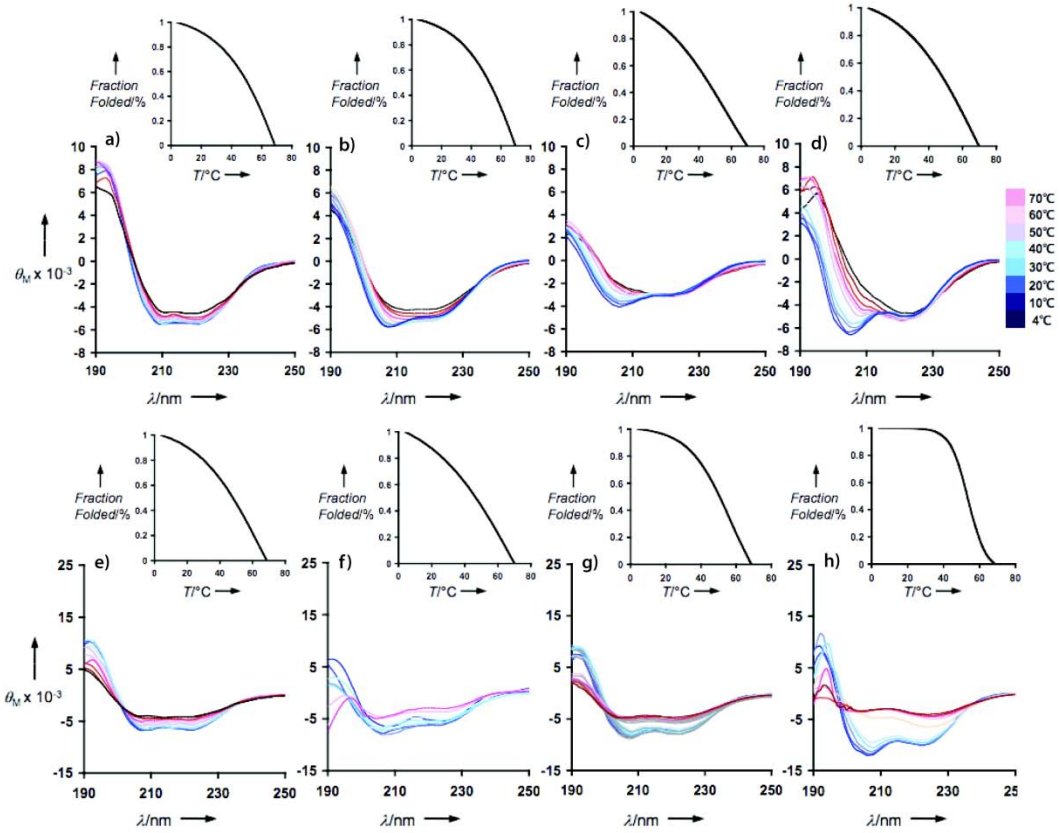

Figure 22. CD wavelength and temperature spectra of a) E_1C, b) E_2C, c) E_3C, d) E_4C, e) CE_1, f) CE_2, g) CE_3, and h) CE_4.

performing the secondary structure and melt analysis. Although nearly identical in composition, the E_nC and CE_n diblocks differ in secondary structure and exhibit distinct temperature dependent conformational changes. In the case of all the E_nC library members, a random like structure is observed at low temperatures (with the exception of E_1C, Figure 6a), which then shifts into a predominantly helical or beta conformation for E_2C and E_3C or E_4C, respectively (Figure 22b-d). By contrast, the CE_n library members reveal an overall structure that appears to be predominantly helical at low temperatures. In general, the overall helical conformation is maintained for most CE_n block polymers, while for CE_4, the minima at 225 nm is dominant over the 208 nm minima indicative of a more beta like structure (Figure 22). Moreover each library member exhibits a distinct melting temperature (T_m) spanning from 54 to 84 ^oC. In general the E_nC diblocks exhibited higher T_m's relative to their respective CE_n (Figure 22). In the case of the diblocks bearing four repeats of elastin, the E_4C (68^oC) reveals a higher T_m than the CE_4 by 14^oC, while for the dibocks with three elastin repeats, both possess an identical T_m of 57^oC. For the diblocks with two elastin repeats, the E_2C (80^oC) shows a higher T_m by 16^oC in comparison to the CE_2. The dibocks with one elastin repeat reveals the largest difference in T_m in which E_1C (84^oC) exhibits an 18^oC higher melt than CE_1. This behavior is interesting in light of the observation that both E_1C and CE_1 illustrate similar helical initial structures. These data confirm that on the microscale, the E_nC and CE_n diblocks behave differently even though they may be compositionally identical.

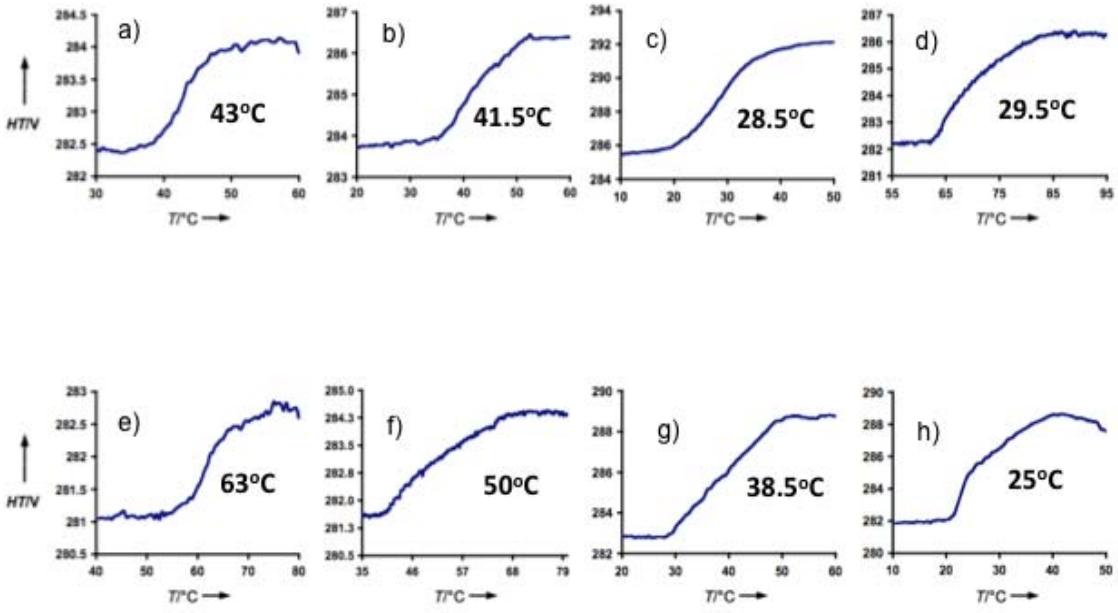

Figure 23. CD HT spectra showing T_t of a) E_1C, b) E_2C, c) E_3C, d) E_4C, e) CE_1, f) CE_2, g) CE_3, and h) CE_4.

The transition temperature (T_t) of each library member was also measured via CD (Figure 23). The HT voltage at the photomultiplier tube could be used to monitor turbidity since it increases with absorbance in CD [15-17]. Each block polymer revealed a different T_t; specifically all values for E_mC were different from its corresponding CE_m counterpart.

This illustrated that the orientation of the blocks are important in terms of supramolecular assembly. For the E_mC and CE_m libraries, as the E domain was shortened, an overall increase in T_t was observed with the exception of E_3C and E_4C (Figure 23). Thus as expected truncating the E domain raised the T_t.

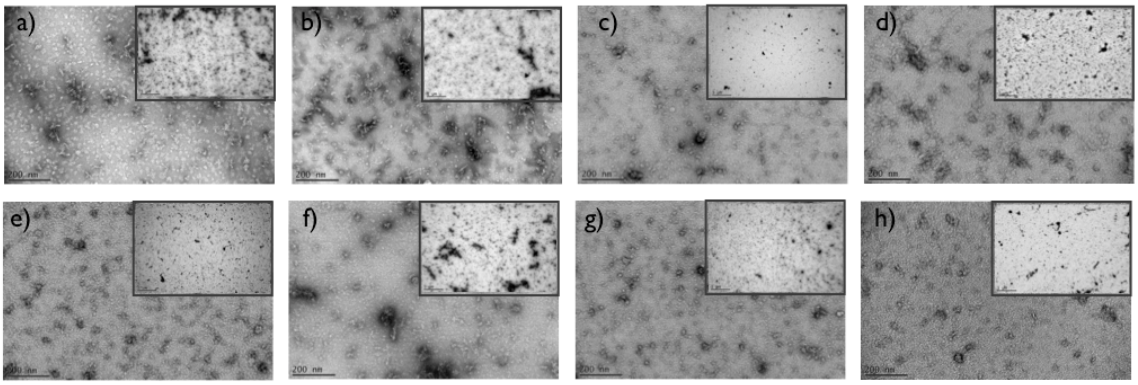

Figure 24. TEM of a) E_1C, b) E_2C, c) E_3C, d) E_4C, e) CE_1, f) CE_2, g) CE_3, and h) CE_4. Scale bars represent 200 nm an insets represent 1 μm.

To visualize the supramolecular assemblies, TEM analysis was performed on the libraries (Figure 24). In the case of the E_nC series, the particles ranged from 20.9 ± 2.6 nm to 29.7 ± 4.9 nm in which the particle size decreased as the E domain was truncated. For the CE_n series, the particles ranged from 23.7 ± 4.4 nm to 27.8 ± 4.1 nm. In this series, the size differences did not correspond to the E domain length. This could be attributed to the N-terminal C domain being dominant in the supramolecular assembly. This work is being written up for publication.

References:

(1) Urry, D. W.; Hugel, T.; Seitz, M.; Gaub, H. E.; Sheiba, L.; Dea, J.; Xu, J.; Parker, T. *Philosophical Transactions of the Royal Society of London Series B-Biological Sciences* **2002**, *357*, 169.

(2) Urry, D. W.; Trapane, T. L.; Prasad, K. U. *Biopolymers* **1985**, *24*, 2345.

(3) Guo, Y.; Kammerer, R. A.; Engel, J. *Biophysical Chemistry* **2000**, *85*, 179.

(4) Guo, Y.; Bozic, D.; Malashkevich, V. N.; Kammerer, R. A.; Schulthess, T.; Engel, J. *EMBO J* **1998**, *17*, 5265.

(5) Ozbek, S.; Engel, J.; Stetefeld, J. *Embo Journal* **2002**, *21*, 5960.

(6) Haghpanah, J. S.; Yuvienco, C.; Civay, D. E.; Barra, H.; Baker, P. J.; Khapli, S.; Voloshchuk, N.; Gunasekar, S. K.; Muthukumar, M.; Montclare, J. K. *Chembiochem* **2009**, *10*, 2733.

(7) Urry, D. W.; Luan, C. H.; Peng, S. Q. In *Molecular Biology and Pathology of Elastic Tissues* 1995; Vol. 192, p 4.

(8) Baker, P. J.; Haghpanah, J. S.; Montclare, J. K. *Elastin Based Protein Polymers*; Oxford University Press: Oxford, 2008.

(9) Haghpanah, J. S.; Yuvienco, C.; Roth, E.; Liang, A.; Tu, R. S.; Montclare, J. K. *Molecular BioSystems* **2010**, *in press.*

(10) Gunasekar, S. K.; Asnani, M.; Limbad, C.; Haghpanah, J. S.; Hom, W.; Barra, H.; Nanda, S.; Lu, M.; Montclare, J. K. *Biochemistry* **2009**, *48*, 8559.

(11) Walters, M. R. *Endocrinology Review* **1992**, *13*, 719.

(12) Bouillon, R.; Okamura, W. H.; Norman, A. W. *Endocrinology Review* **1995**, *16*, 200.

(13) Simmerman, H. K. B.; Kobayashi, Y. M.; Autry, J. M.; Jones, L. R. *Journal of Biological Chemistry* **1996**, *271*, 5941.
(14) Greenfield, N. J. *Methods in Enzymology* **2004**, *383*, 282.
(15) Klaikherd, A.; Nagamani, C.; Thayumanavan, S. *Journal of the American Chemical Society* **2009**, *131*, 4830.
(16) Aathimanikandan, S. V.; Savariar, E. N.; Thayumanavan, S. *Journal of the American Chemical Society* **2005**, *127*, 14922.
(17) Arvinte, T.; Bui, T. T. T.; Dahab, A. A.; Demeule, B.; Drake, A. F.; Elhag, D.; King, P. *Analytical Biochemistry* **2004**, *332*, 46.